

**PCCP****The energy level of the Fe²⁺/³⁺-transition in BaTiO₃ and SrTiO₃ single crystals**

Journal:	<i>Physical Chemistry Chemical Physics</i>
Manuscript ID	CP-ART-12-2018-007872.R1
Article Type:	Paper
Date Submitted by the Author:	15-Feb-2019
Complete List of Authors:	Suzuki, Issei; Tohoku University, Gura, Leonard; Fritz-Haber-Institut der Max-Planck-Gesellschaft Klein, Andreas; Darmstadt University of Technology, Materials Science

SCHOLARONE™
Manuscripts

Cite this: DOI: 10.1039/xxxxxxxxxx

The energy level of the Fe^{2+/3+}-transition in BaTiO₃ and SrTiO₃ single crystals[†]

Issei Suzuki,^{*‡} Leonard G. Gura,[¶] and Andreas KleinReceived Date
Accepted Date

DOI: 10.1039/xxxxxxxxxx

www.rsc.org/journalname

An approach to determine the defect energy levels of the Fe impurities in BaTiO₃ and SrTiO₃ single crystals using electrical conductance measurements is presented. The defect levels are obtained from the dependence of the activation energy of electrical transport on the oxygen vacancy concentration, which is varied by stepwise re-oxidation of a reduced sample. An energy level at 0.7–0.8 eV below the conduction band minimum E_{CB} is identified for BaTiO₃, which can be assigned to the Fe^{2+/3+}-transition in good agreement with literature. In contrast, the conductivity of Fe-doped SrTiO₃ does not show a defect energy level in the upper half of the band gap, indicating that the Fe^{2+/3+}-transition in SrTiO₃ is near the conduction band minimum. The often reported alignment of defect energy levels, which is fulfilled for the Fe^{3+/4+}-transition in BaTiO₃ and SrTiO₃, does not hold for the Fe^{2+/3+}-transition in these compounds. This limits the applicability of Fe-doped SrTiO₃ as a model system for studying resistance degradation in acceptor-doped high-permittivity dielectrics.

1 Introduction

The increase of insulation resistance of high-permittivity dielectrics (resistance degradation), which occurs at elevated temperatures under applied electric field and which is governed by oxygen vacancy migration at temperatures above $\sim 100^\circ\text{C}$,^{1,2} remains a major obstacle for high-temperature application of multilayer ceramic capacitors.^{3–6} Acceptor-doped BaTiO₃ is widely used for such applications. The increase of the leakage current of such capacitors is well described by assuming internal field-driven rearrangement of oxygen vacancies.^{1,2} A strong chemical reduction of the dielectric near the cathode, which has been observed by different techniques,^{7–11} is likely related to a removal of oxygen from the dielectric. This must occur at the anode under operation conditions.

The change of oxygen content of a material by oxygen extraction and incorporation is affected by ionic space charge regions,¹² which are determined by the difference in Fermi energy in the bulk and at the surface. The latter is determined by the Schottky

barrier at the electrode interface and can be measured directly using photoelectron spectroscopy.¹³ The Fermi level in the bulk is, on the other hand, determined by the concentrations and energy levels of defects, such as (un)intentional impurities (dopants), and intrinsic defects, such as cation and anion vacancies or interstitials.

The energy levels of defects are related to the change of valence. Depending on the valence relative to the host site (lattice or interstitial position), an impurity can act as an electron source (donor) or trap (acceptor). The controlled doping of semiconductors is the basis for almost all electronic devices and relies on shallow defect states, which can be easily ionized at room temperature.¹⁴ As such materials are good electronic conductors, the energy levels of the defects can be determined by electrical transport measurements, for example using the Hall effect.¹⁵ Oxygen vacancies in BaTiO₃ and SrTiO₃ are also shallow defects, with energy levels near the conduction band minimum.^{16–19}

In contrast to this, transition-metal impurities generate deep defect levels.^{14,20–22} In electronically conducting materials, the energy levels of such defects can still be identified using electrical measurements, such as deep level transient spectroscopy (DLTS) or admittance spectroscopy.^{15,23} In dielectric materials, such as BaTiO₃, these techniques cannot be applied due to their low electrical conductivity.

Transition-metal impurities cannot be avoided in high-permittivity dielectrics. In BaTiO₃, for example, Fe is the most abundant impurity, which occurs in concentrations between 5 and

Technische Universität Darmstadt, Institute of Materials Science, 64287 Darmstadt, Germany. E-mail: issei.suzuki@tohoku.ac.jp

[†] Electronic Supplementary Information (ESI) available: Additional conductivity measurements of BaTiO₃; Impurity analysis of BaTiO₃ single crystals using GMDS. See DOI: 10.1039/cXCP00000x/

[‡] Present address: Institute of Multidisciplinary Research for Advanced Materials (IMRAM), Tohoku University, 2-1-1 Katahira Aoba-ku, Sendai 980-8577, Japan

[¶] Present address: Fritz-Haber-Institute of the Max-Planck-Society, Faradayweg 4-6, 14195 Berlin, Germany

100 ppm,^{24–26} corresponding to $0.3\text{--}6 \cdot 10^{18}$ Fe atoms per cm^3 . These impurities participate, for example, in the photorefractive effect of BaTiO_3 .²⁵ Other transition-metals, such as Mn, are intentionally inserted in BaTiO_3 ceramics in order to reduce the leakage current in multilayer ceramic capacitors.³

Regarding the energy levels of Fe in BaTiO_3 and SrTiO_3 , the $\text{Fe}^{3+/4+}$ -transition is well established in both materials.^{17,27–32} The charge transition occurs at an energy of 0.8–0.9 eV above the valence band maximum. In contrast to this, the $\text{Fe}^{2+/3+}$ -transition is considered only in BaTiO_3 with an energy level of ~ 2.4 eV above the valence band maximum.^{27,28,33} There is, however, also evidence from Mössbauer spectroscopy and infrared absorption for the presence of Fe^{2+} , either in reduced or in La co-doped Fe-doped SrTiO_3 .^{34–36} An impedance study of degraded Fe-doped SrTiO_3 single crystals by Bayer et al. indicated the presence of an electron trap in the cathode region with an activation energy of 1.01 eV.³⁷ If this trap is related to the $\text{Fe}^{2+/3+}$ -transition, it would be at a similar energy as the same transition in BaTiO_3 . Such an alignment of defect energy levels has been reported for other systems, such as transition-metal impurities in III-V semiconductors,^{20–22} hydrogen impurities³⁸ and oxygen vacancies³⁹ and would therefore not be unexpected.

In this study, we present an approach to determine the defect energy levels using electrical conductance measurements. The defect level of Fe in a BaTiO_3 single crystal is obtained from the dependence of the activation energy of transport on the oxygen vacancy concentration. The latter is varied by stepwise re-oxidation of a reduced sample. An energy level at 0.7–0.8 eV below the conduction band minimum E_{CB} is identified, being in good agreement with literature on the $\text{Fe}^{2+/3+}$ transition. In contrast, the conductivity of Fe-doped SrTiO_3 does not show a defect energy level in the upper half of the band gap.

2 Defect Model and Activation Energy

The defect chemistry of acceptor-doped BaTiO_3 is extensively described in literature.^{24,27,32,40–42} The relevant defect reactions are the oxygen exchange reaction, electron-hole pair generation and the ionization reactions of the acceptor. Partial de-ionization of oxygen vacancies into a singly charged and a neutral charge state has also been considered. In the case of Fe acceptors, which is the dominant impurity in the studies samples, three different valencies, 4+, 3+ and 2+ with charge transitions of $E_{\text{A}1} = 0.8$ eV for the $\text{Fe}^{3+/4+}$ - and $E_{\text{A}2} = 2.4$ eV for the $\text{Fe}^{2+/3+}$ -transition are considered, respectively.^{17,27,28} The ionisation energies of the acceptors are given with respect to the valence band maximum E_{VB} .

In order to calculate the electrical conductivity of the samples, one further requires the concentrations and mobilities of the different defects. As our experiments are not performed in controlled oxygen partial pressure, we take the oxygen vacancy concentration $c(\text{V}_{\text{O}}^{\bullet\bullet})$ as a variable. The concentrations of electrons (n), holes (p), neutral (Fe^{4+}), singly- (Fe^{3+}) and doubly-charged (Fe^{2+}) acceptors depend on the Fermi energy according to:

$$n = N_{\text{C}} \cdot \exp((E_{\text{CB}} - E_{\text{F}})/k_{\text{B}}T) \quad (1)$$

$$p = N_{\text{V}} \cdot \exp((E_{\text{F}} - E_{\text{VB}})/k_{\text{B}}T) \quad (2)$$

$$c(\text{Fe}^{2+}) = c(\text{Fe}) \cdot \frac{1}{1 + g_{\text{A}} \cdot \exp((E_{\text{A}2} - E_{\text{F}})/k_{\text{B}}T)} \quad (3)$$

$$c(\text{Fe}^{3+}) = c(\text{Fe}) \cdot \frac{1}{1 + g_{\text{A}} \cdot \exp((E_{\text{A}1} - E_{\text{F}})/k_{\text{B}}T)} - c(\text{Fe}^{2+}) \quad (4)$$

$$c(\text{Fe}^{4+}) = c(\text{Fe}) - c(\text{Fe}^{3+}) - c(\text{Fe}^{2+}) \quad (5)$$

Here $N_{\text{C},\text{V}}$ are the effective density of states in the conduction and valence band and $g_{\text{A}} = 2$ is the spin degeneracy factor. The former are obtained from the expression for parabolic energy bands using effective masses for electrons ($m_e^* = 5 \cdot m_e$) and holes ($m_h^* = m_e$), which correspond to effective densities of states in the conduction band of $N_{\text{C}} = 5.50 \cdot 10^{20} \text{ cm}^{-3}$ and in the valence band of $N_{\text{V}} = 4.92 \cdot 10^{19} \text{ cm}^{-3}$, respectively. We have a band gap of 3 eV, which corresponds to the magnitude at 200 °C.

The Fermi level position E_{F} and defect concentrations as a function of oxygen vacancy concentration can then be obtained by solving the charge neutrality condition

$$2 \cdot c(\text{V}_{\text{O}}^{\bullet\bullet}) + p = 2 \cdot c(\text{Fe}_{\text{Ti}}^{\prime\prime}) + c(\text{Fe}_{\text{Ti}}^{\prime}) + n \quad (6)$$

for each oxygen vacancy concentration $c(\text{V}_{\text{O}}^{\bullet\bullet})$. The results obtained for an Fe concentration of $3 \cdot 10^{17} \text{ cm}^{-3}$ are shown in Fig. 1a) and b). In this calculation, the energy levels of the $\text{Fe}^{2+/3+}$ -transition has been set to 0.8 eV below the conduction band minimum in order to be comparable to the experimental results reported below. The energy level of the $\text{Fe}^{3+/4+}$ -transition has been set to 0.9 eV above the valence band maximum in order to distinguish the activation energies related to the two levels. The results of the calculations are comparable to those reported by Wechsler and Klein and by Maier and Randall for differently doped BaTiO_3 .^{27,32}

The mobilities of electrons in dependence on temperature is given by Ihrig⁴³ and the oxygen vacancy mobility from diffusivity data reported by Kessel and coworkers.⁴⁴ The latter have also been used by Maier and Randall.³²

$$\mu_e = 8080 \cdot T^{-1.5} \cdot \exp(-0.021/k_{\text{B}}T) \quad (7)$$

$$\mu_h = \frac{1}{2} \cdot \mu_e \quad (8)$$

$$\mu_{\text{V}_{\text{O}}^{\bullet\bullet}} = \frac{ze}{k_{\text{B}}T} \cdot D_{\text{V}_{\text{O}}} = \frac{2e}{k_{\text{B}}T} \cdot 6.4 \cdot 10^{-3} \cdot \exp(-0.7/k_{\text{B}}T) \quad (9)$$

Following Chan et al.⁴⁵ we estimate the hole mobility, which is not relevant in this work as the hole conductivity does not contribute significantly to the conduction in the measured samples, as half the electron mobility. The total conductivity of the sample is finally obtained by summing up all three contributions:

$$\sigma_{\text{tot}} = qn\mu_e + qp\mu_h + 2qc(\text{V}_{\text{O}}^{\bullet\bullet})\mu_{\text{V}_{\text{O}}^{\bullet\bullet}} \quad (10)$$

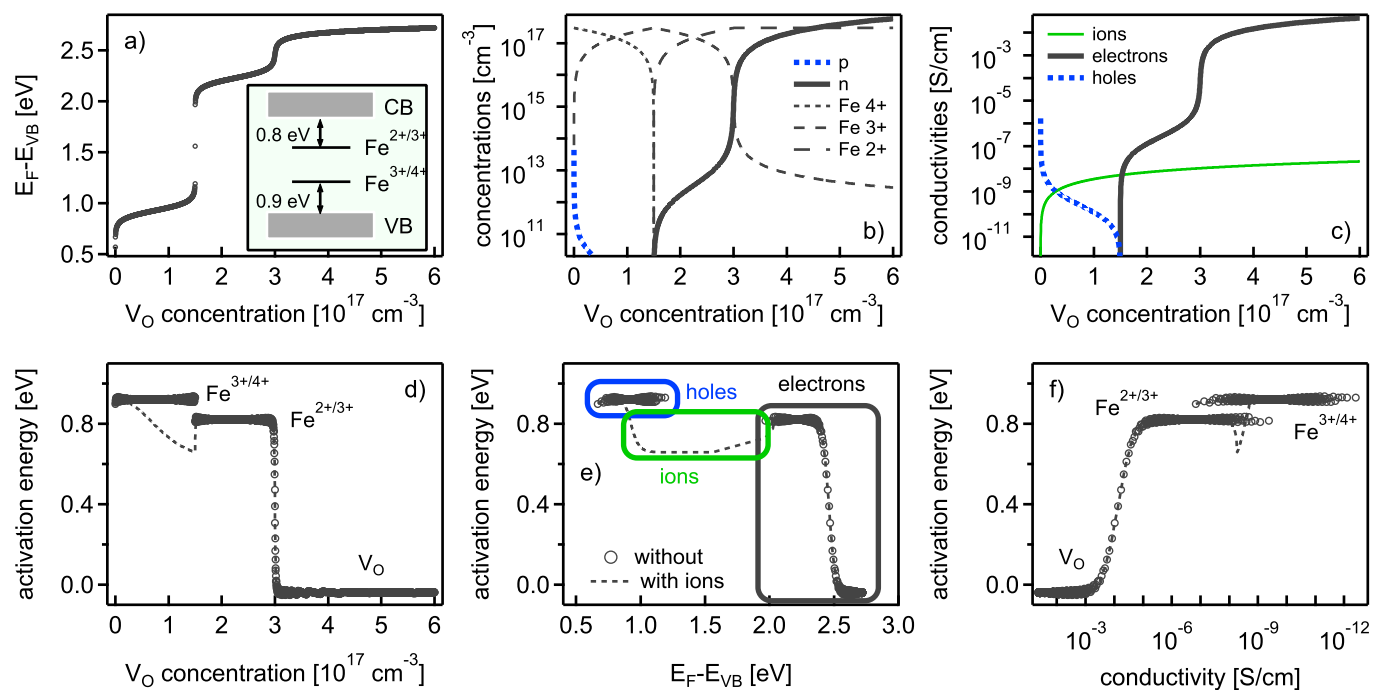


Fig. 1 Fermi level position (a), defect concentrations (b), partial conductivities (c) as a function of oxygen vacancy concentration at 200 °C. The Fe concentration is set to $3 \cdot 10^{17} \text{ cm}^{-3}$, the band gap to 3 eV and energy levels of the $\text{Fe}^{3+/4+}$ and $\text{Fe}^{2+/3+}$ transitions to 0.9 eV above the valence band maximum and to 0.8 eV below the conduction band minimum, respectively. The activation energy is shown vs. oxygen vacancy concentration in (d), vs. Fermi level position in (e), and vs. conductivity in (f). Circles and dashed lines in (d)–(f) correspond to activation energies of conductivity without and with ionic conductivity included.

In principle, it would be necessary to add polaron transport by hopping of electrons between the Fe centers. As the concentration of Fe is rather low in the studied samples ($c(\text{Fe}) = 3 \cdot 10^{17} \text{ cm}^{-3}$), this contribution can be neglected. The resulting partial conductivities are displayed in Fig. 1c).

The activation energy, which is shown in Fig. 1d)–e) in dependence oxygen vacancy concentration, Fermi level and conductivity, respectively, are obtained by calculating the defect concentrations and carrier mobilities at two different temperatures, 200 and 220 °C. The activation energy clearly shows three different regions: At low, medium and high oxygen vacancy concentration, the activation energy is determined by the $\text{Fe}^{3+/4+}$ and the $\text{Fe}^{2+/3+}$ transitions and by the oxygen vacancies, respectively. The activation energies of the former two are exactly the energy differences between the transition levels and the valence and conduction band, respectively. The negative activation energies for strongly reduced samples result from the fact that the oxygen vacancies are rather shallow donors, which are completely ionized at the measurement temperature. The concentration of ionized oxygen vacancies, and therefore also that of the electrons, does therefore not depend on temperature. The activation energy of electrical conductivity is then completely determined by the temperature dependence of electron mobility, which is given by equation 7. As the carrier mobility decreases with increasing temperature, a negative activation energy results.

3 Experimental details

Nominally undoped BaTiO_3 and 0.05 wt.% Fe-doped SrTiO_3 single crystals with a dimension of $5 \times 5 \times 0.5 \text{ mm}^3$ were purchased from Alineason Materials Technology GmbH, Frankfurt, Germany and from MaTeck GmbH, Jülich, Germany, respectively. Both crystals have [100] orientation. The BaTiO_3 samples had a slightly yellowish appearance while the Fe-doped SrTiO_3 crystals exhibit a light brownish colour. Impurity concentrations of the BaTiO_3 crystals were measured by using Glow Discharge Mass Spectrometry (GDMS). The most relevant impurity concentrations are given in Table 1. A complete list of concentrations is included in the supplementary information.[†] The Fe concentration in SrTiO_3 corresponds to $2.75 \cdot 10^{19} \text{ cm}^{-3}$.

Table 1 Concentrations obtained from glow discharge mass spectrometry (GDMS) of the major impurities in the BaTiO_3 single crystals used in the present study. Concentrations of other elements are available in the supplementary information.[†]

element	c in ppm	c in cm^{-3}
Fe	4.7	$3.0 \cdot 10^{17}$
Al	0.26	$3.5 \cdot 10^{16}$
Mn	0.11	$7.2 \cdot 10^{15}$
Mg	0.66	$9.8 \cdot 10^{16}$
Ni	0.36	$2.2 \cdot 10^{16}$

The samples for the electrical measurement were prepared as follows; the crystals were sonicated in acetone, isopropanol and

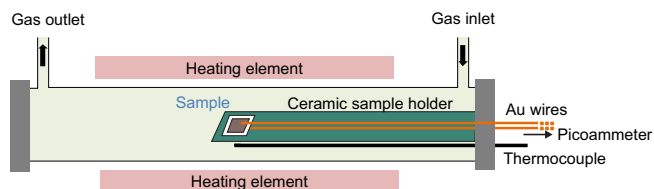


Fig. 2 Schematic illustration of the setup for simultaneous re-oxidation and conductivity measurement. A Au wire is used for the contact to the sample's surface.

ethanol for 5 mins each. Subsequently, the crystals were then equilibrated at 900 °C for 12 h in air and quenched to room temperature with a high cooling rate of ~ 60 K/s. No cracks were detected after the quench. The first BaTiO₃ sample (sample 1) was then coated with Pt electrodes of 50 nm thickness on both top and bottom surfaces by DC magnetron sputtering. The crystal was then reduced by annealing in vacuum at $\sim 5 \cdot 10^{-5}$ Pa at 700 °C for 12 h resulting in a slightly bluish appearance. In-situ X-ray photoelectron spectroscopy (XPS) measurements of crystals treated this way exhibit a Fermi energy close to the conduction band minimum.⁴⁶ A second BaTiO₃ crystal (sample 2) was reduced by annealing in glass tube with 5% H₂ and 95% Ar mixture flow of 60 sccm at 600 °C for 12 h. SrTiO₃ crystals were reduced by heating in H₂/Ar at 1000 °C for 14 hours. Pt electrodes were deposited on both surfaces afterwards. The reducing conditions for SrTiO₃ were set in order to obtain sufficiently high electrical conductivity. The stronger reducing conditions required for SrTiO₃ as compared to BaTiO₃ are reasonable due to the higher Fe concentration.

The re-oxidation and electrical measurement of the samples were simultaneously conducted in the furnace illustrated in Fig. 2. In order to re-oxidize the samples, they were heated up and cooled down repetitively with a rate of 2.5 K/min. Between heating and cooling, the samples were stored at the maximum temperature for a couple of minutes. The dc conductivity of the samples was continuously recorded with a Keithley 6487 picoammeter/voltage source (Keithley Instruments Inc., Ohio, USA), which was connected to the sample surfaces with a mechanically attached gold wire. The voltage applied was ranging from 10 to 100 mV depending on the resistivity of the sample. A low voltage was chosen to avoid polarization of the sample during measurement.

4 Results and Discussion

4.1 BaTiO₃

Figure 3 shows the Arrhenius plot of the conductivity measured during consecutive heating and cooling of a BaTiO₃ single crystal reduced by heating in vacuum (sample1). At the beginning, the sample exhibits a conductivity of $\sim 10^{-2}$ S/cm. Taking a carrier mobility of 0.5 cm²/Vs, this corresponds to an electron concentration of $\sim 10^{17}$ cm⁻³, indicating that the oxygen vacancy concentration is only slightly higher than the Fe concentration. The sample is clearly n-type (Samples showing a conductivity which decreases/increases with increasing oxygen content are denominated as n-/p-type as common in defect chemistry and confirmed

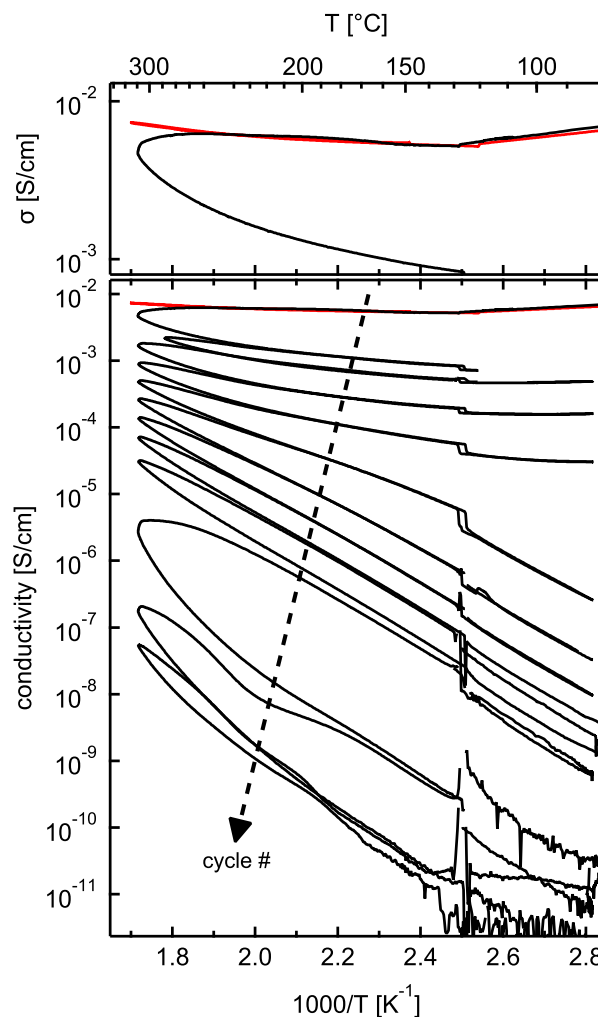


Fig. 3 Arrhenius plot of the conductivity of a BaTiO₃ single crystal reduced by heating in vacuum (sample1). The first two cycles are shown in a magnified view at the top. The first cycle was conducted in vacuum $\sim 1 \cdot 10^{-5}$ Pa and is shown in red. All subsequent cycles were performed at ambient pressure in an atmosphere containing 99% N₂ and 1% O₂ and are shown in black.

by Seebeck measurements⁴⁷) and dominated by electron conduction, which agrees with the high Fermi energy measured by XPS of similarly treated samples.⁴⁶

The first cycle was conducted in vacuum ($\sim 1 \cdot 10^{-5}$ Pa). The conductivity during heating in vacuum is identical to the one measured during cooling, indicating that the oxygen vacancy concentration does not change during the cycle. Hence no oxygen was incorporated during the temperature cycle. For temperatures < 128 °C, which is the temperature at which the ferroelectric polarization of the crystal vanishes, the conductivity decreases with increasing temperature. This corresponds well to the negative activation energy in Fig. 1(d-f), which is a consequence of the temperature dependence of carrier mobility. In the respective temperature region, the conductivity also exhibits a power law dependence with a temperature exponent of -1.8 , which roughly agrees with the expected dependence from Eq. 7. Contrastingly, for temperatures > 128 °C, the conductivity increases with increas-

ing temperature. A similar change in slope has been reported by Berglund and Baer.¹⁶ However, the temperature dependence of mobility according to Eq. 7 is expected to prevail particularly above the Curie temperature.^{32,44} Increasing the concentration of electronic carriers is also not expected to cause the change in slope, as all oxygen vacancies should be ionized already at room temperature due to their low ionization energy.

The change in slope is obviously related to the phase transition from the tetragonal ferroelectric to the cubic paraelectric phase. Measurements performed on reduced Fe-doped SrTiO₃ (see section 4.2) show a negative temperature coefficient at all temperatures, corresponding to the behaviour of BaTiO₃ in the ferroelectric phase. The origin of the behaviour of reduced BaTiO₃ is not clear yet. Schottky barriers at the contacts, which depend on polarization,⁴⁸ could contribute to the effect and may explain the positive temperature coefficient in the paraelectric phase. However, Schottky barriers at the electrode interface do not seem to play a role in the measurements. This will be addressed more extensively in section 4.2.

All subsequent cycles were performed in ambient pressure in an atmosphere containing 99% N₂ and 1% O₂. During the first oxidation cycle, the conductivity follows the course of the vacuum cycle during heating up to 250°C. For $T > 250^\circ\text{C}$, the conductivity starts to increase more slowly with temperature before it even decreases with temperature. During the cooling, the conductivity is substantially lower than the one during heating up. The decrease of conductivity is a clear indication for oxygen incorporation into the sample, which decreases the electron concentration and therefore the conductivity. In addition to the decrease of conductivity, the slope of the curve at lower temperature also increased. The activation energy determined at 200°C increased from ~ 0.08 to ~ 0.16 eV.

In the following, the sample was repetitively re-oxidized in the N₂/O₂ atmosphere. In every measurement cycle the conductivity increases linearly with increasing temperature up to $\sim 250^\circ\text{C}$. At higher temperatures the conductivity increases slower and then decreases, resulting in a significantly lower conductivity during cooling. With increasing cycle number, the conductivity continuously decreases. Concurrently, the activation energy increases with decreasing conductivity. To ensure the reproducibility of this re-oxidation experiment, an additional measurement was conducted on a second sample, which was reduced by heating in H₂/Ar. The resulting behaviour is comparable (see Fig. S1 in the supplementary information[†]).

Up to temperatures of $\sim 250^\circ\text{C}$, the conductivity during heating follows the behaviour during cooling in the preceding cycle. This suggests a homogeneous distribution of oxygen vacancies at $T < 250^\circ\text{C}$. Such a homogeneous distribution requires that diffusion is much faster than oxygen incorporation, which might be justified as oxygen is mobile already at 200°C.³² The time τ to achieve an almost homogeneous distribution of oxygen in a slab of thickness $2L$ is then given by $\tau = L^2/2D_0^\delta$, where D_0^δ is the chemical diffusivity of oxygen, which is connected to the vacancy diffusivity $D_{V_O^{\bullet\bullet}}$ via:¹²

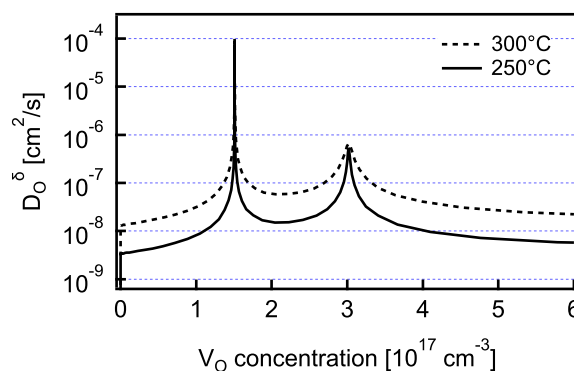


Fig. 4 Chemical diffusion coefficient of oxygen in BaTiO₃ with an Fe impurity concentration of $3 \cdot 10^{17} \text{ cm}^{-3}$. The curves are calculated at 250 and 300°C using Eq. 11.

$$D_0^\delta = D_{V_O^{\bullet\bullet}} \cdot \frac{c(V_O^{\bullet\bullet})}{c(O_O)} \cdot \frac{\partial \ln p(O_2)}{2 \partial \ln c_O} \quad (11)$$

The result of the calculation of D_0^δ for $T = 250$ and 300°C is shown in Fig. 4 as a function of oxygen vacancy concentration. For high oxygen vacancy concentration, D_0^δ approaches the value of $3 \cdot D_{V_O^{\bullet\bullet}}$ ($3.5 \cdot 10^{-9} \text{ cm}^2/\text{s}$ at 250°C and $1.3 \cdot 10^{-8} \text{ cm}^2/\text{s}$ at 300°C according to Eq. 9), in agreement with the expression derived by de Souza.¹² D_0^δ exhibits pronounced maxima at $c(V_O) \approx c(\text{Fe})$ and $c(V_O) \approx \frac{1}{2}c(\text{Fe})$ and is $> 10^{-8} \text{ cm}^2/\text{s}$ for a wide range of concentrations around these values. Therefore, the homogenization time is estimated to be $\tau < 8.6$ h. Considering the slow heating and cooling rates of 2.5 K/min, the fact that homogenization already occurs at temperatures above 250°C and that oxygen vacancy concentrations are close to the Fe concentration, it appears reasonable to assume a largely homogeneous distribution of oxygen vacancies in the sample.

The calculation of the chemical diffusivity does not take electron/hole trapping into account, which can substantially slow down the diffusion of ionic species if their concentration becomes too low to charge balance the ionic motion.⁴⁹ In Fe-doped SrTiO₃, the effect becomes pronounced at high oxygen pressure and low temperature when the oxygen vacancy concentration is low compared to the Fe concentration.^{49,50} The situation in the presented experiments is different as the regime of high oxygen activity is not reached. The activation energies we extract are for concentrations of oxygen vacancies larger than half the Fe concentration (n-type regime). As shown in Fig. 1, the electron concentration at 200°C is sufficient to charge balance oxygen ion transport. Hence, the ambipolar diffusion coefficient is more or less the same as that of the oxygen vacancies. Moreover, our data implicate that oxygen incorporation and distribution takes place at $T > 200^\circ\text{C}$, where the electron concentration should be higher.

Another important question is how much ionic conductivity contributes to the measured conductivity. Platinum electrodes are considered as being oxygen blocking. But, oxygen incorporation may still take place at the triple phase boundaries at the edges of Pt contacts. Using the same sample geometry, we could record time independent currents with dc voltages for Y-stabilized ZrO₂

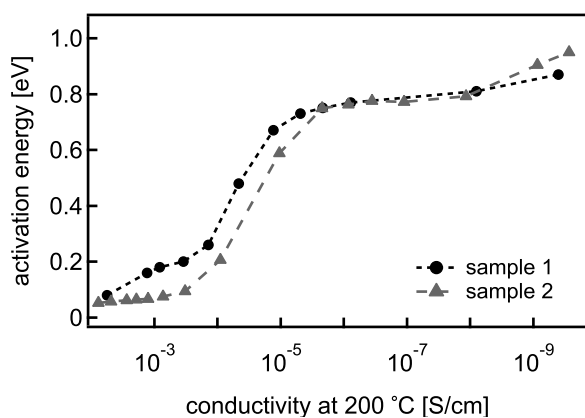


Fig. 5 Activation energy vs. electrical conductivity of the 2 studied BaTiO₃ crystals. The conductivity data for sample 1 are shown in Fig. 3, those of sample 2 in Fig. S1 in the supporting information.[†]

(YSZ) with Pt electrodes. The current through YSZ is only possible by ionic transport. Hence, a contribution of ionic transport to the current through the crystal can not be excluded. The magnitude of the measured current is, however, much higher than expected for ionic conductivity. The calculation shown in Fig. 1(c) reveals an ionic conductivity at 200 °C of 10^{-9} – 10^{-8} S/cm. Such low conductivities are only observed during the very last cycles in Fig. 3. Even at this low conductivity, the conductivity is not necessarily determined by ionic motion.

The activation energies are determined from linear approximation of $\ln(\sigma T)$ in the temperature range 150–200 °C. The results obtained for the 2 investigated BaTiO₃ samples are shown in Fig. 5 as a function of conductivity at 200 °C. Both samples show a very similar behaviour with a rise of the activation energy in the conductivity range $S = 10^{-3}$ – 10^{-5} S/cm. This corresponds well to the dependence calculated in section 2, indicating that the experimental approach is valid for the determination of the energy level of defects. The activation energy exhibits a clear plateau at ~ 0.8 eV. Within the assumed defect model this plateau can be assigned to the Fe^{2+/3+}-transition. The derived energy level is in good agreement with the values reported in literature.^{17,27,28}

4.2 SrTiO₃

Hall effect measurements in van der Pauw geometry of reduced SrTiO₃ crystals revealed electron concentrations and mobilities of $\sim 10^{18}$ cm⁻³ and ~ 6 cm²/Vs, respectively. Assuming that the electron concentration is equal to $c(V_{\text{O}}^{\bullet\bullet}) - c(\text{Fe}_{\text{Ti}}^{\prime\prime})$, the oxygen vacancy concentration is less than 10% higher than the Fe concentration of $2.75 \cdot 10^{19}$ cm⁻³.

The evolution of electrical conductivity measured in parallel plate geometry with Pt electrodes is shown in Fig. 6 in the course of stepwise re-oxidation. In general higher temperatures are required to re-oxidize the Fe-doped SrTiO₃ in comparison to the unintentionally doped BaTiO₃. This is reasonable as the total amount of oxygen to be incorporated is much higher due to higher dopant concentration.

As for the BaTiO₃ crystals, the first cycle shows a conductivity of $\sim 10^{-2}$ S/cm and a negative temperature coefficient. How-

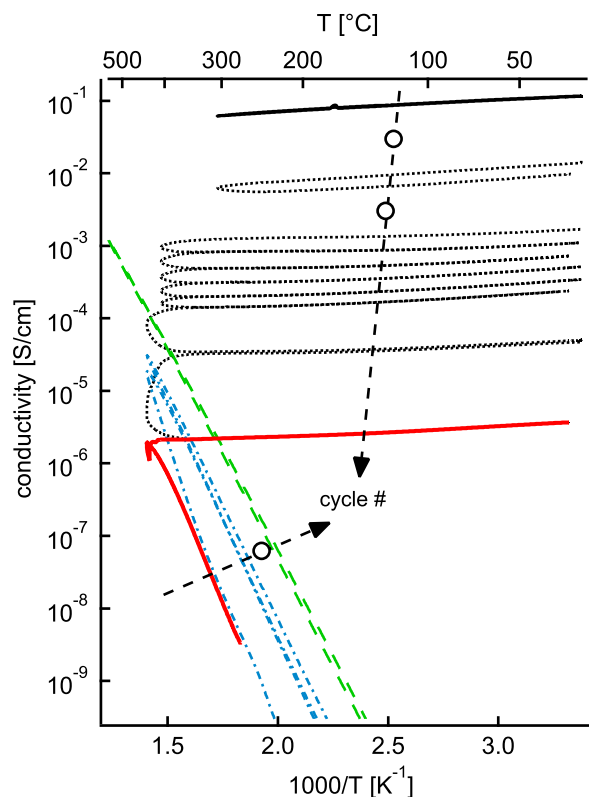


Fig. 6 Arrhenius plot of the conductivity of a reduced SrTiO₃ single crystal. All cycles were performed at ambient pressure in an atmosphere containing 99% N₂ and 1% O₂. The first cycle is shown by a solid black line. Consecutive cycles are shown by dotted black lines. The solid red line shows the two cycles where the conductivity changes from a negative to a positive temperature coefficient. The dash-dotted blue line indicates the cycle recorded just after the transition to semiconducting behaviour. The final cycles are shown by dashed green lines. Open circles indicate additional cycles, which are not displayed.

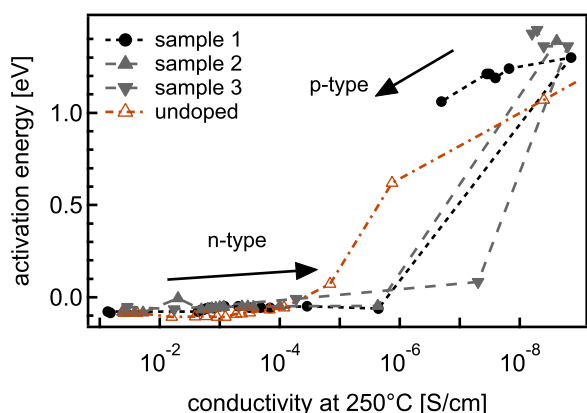


Fig. 7 Activation energy vs. electrical conductivity of SrTiO₃ crystals doped with 0.05 wt.% Fe (sample 1–3) and one nominally undoped crystal. The conductivity data for sample 1 are shown in Fig. 6.

ever, in contrast to BaTiO₃, the negative temperature coefficient of conductivity, which corresponds to a temperature independent carrier concentration, persists with decreasing conductivity. Only at a conductivity of $\sim 2 \cdot 10^{-6}$ S/cm, indicated by the red line in Fig. 6, the sample suddenly changed to a behaviour with a rather high activation energy of > 1.3 eV. This activation corresponds to approximately half of the energy gap. Such an activation is expected when the oxygen vacancy concentration is exactly half of the Fe concentration. Slightly different activation energies will already reduce the activation energy as indicated by the defect model calculations in section 2. In the following cycles, the conductivity increases from cycle to cycle. This indicates that the sample became p-type, which indicates that $c(\text{V}_\text{O}^{\bullet\bullet}) < \frac{1}{2} \cdot c(\text{Fe})$.

The evolution of activation energy in the course of re-oxidation is shown in Fig. 7. The abrupt jump from a negative temperature coefficient to an activation energy corresponding to approximately half the energy gap and a subsequent p-type behaviour is observed in all samples and clearly different from the case of BaTiO₃. The transition from n-type to p-type behaviour seems to be less sharp for the undoped SrTiO₃ sample included in Fig. 7. This has to be taken with caution, however, as there is only a single data point with an intermediate activation energy. In contrast to BaTiO₃, the activation energy of the undoped SrTiO₃ sample does not exhibit a plateau, which is required to clearly identify a defect transition.

The activation energies measured for SrTiO₃ has two main implications: i) ionic conductivity cannot contribute to the measurements. Otherwise the activation energy can't be that high (see Fig. 1); ii) In contrast to BaTiO₃, there is no evidence for the existence of an Fe^{2+/3+} defect level in the band gap of SrTiO₃.

The origin of the different behaviour of the Fe impurity in BaTiO₃ and SrTiO₃ is not clear. It is, however, consistent with literature on defect properties of these materials, which take the Fe^{2+/3+}-transition into account for BaTiO₃^{17,27,28,32} but not for SrTiO₃.^{2,29–31} One possible origin of this discrepancy is the fact that defect properties of SrTiO₃ are mostly investigated at high temperature, where the effect of the second charge transition may not be evident. The present study indicates, however, that the dif-

ferences persists down to room temperature.

The impedance study of degraded Fe-doped SrTiO₃ single crystals by Bayer et al. indicated the presence of an electron trap in the cathode region.³⁷ The cathode region is oxygen depleted due to the field-driven migration of oxygen vacancies towards the cathode in the course of degradation.² By comparison with BaTiO₃, it seems straightforward to associate the observed activation energy of 1.01 eV to the Fe^{2+/3+}-transition. The present study does, however, not support this. A Fe^{2+/3+}-transition at 1.01 eV below the conduction band should also show up as a plateau of the activation energy in the n-type regime. This is evidently not observed.

The present study does not only rule out the Fe^{2+/3+}-transition as origin of the activation energy of 1 eV in the cathode region of degraded crystals, it could not identify an activation of electron transport in reduced Fe-doped SrTiO₃ at all. The presence of the p-n junction and a potentially stronger reduction in the cathode region of the degraded crystals^{10,11} compared to the homogeneously reduced single crystals used in this study may be related to the different behaviour.

There are literature reports providing experimental evidence for the presence of Fe²⁺ in either reduced, or donor (La) co-doped, Fe-doped SrTiO₃.^{34–36} The observation of Fe²⁺ in these studies and the apparent absence of the same in the present study could be consistently explained if the Fe^{2+/3+}-transition is energetically close to the conduction band edge. This is also in good agreement with a recent DFT study by Baker and coworkers.⁵¹ If the Fe^{2+/3+}-transition is energetically close to the conduction band edge in SrTiO₃, they can not be easily distinguished from oxygen vacancies in electrical measurements.

Another difference between SrTiO₃ and BaTiO₃ is the temperature coefficient of conductivity in the cubic phase at higher conductivity, which is positive in the case of BaTiO₃ and negative for SrTiO₃. A negative temperature coefficient is generally not expected in 2-point measurements, as Pt forms a Schottky barrier on these materials.¹³ These are expected to be > 1 eV after oxygen anneal for SrTiO₃⁵² and also for BaTiO₃, due to the negligible band discontinuity between SrTiO₃ and BaTiO₃.^{13,53} The observation of a negative temperature coefficient of conductivity therefore clearly rules out that Schottky barriers at the electrode interface are affecting the measurements.

The reason why ohmic contacts are obtained despite high Schottky barriers for electrons may lie in the Schottky barrier itself. As oxygen vacancies are mobile in the heated samples, they will accumulate adjacent to the interface and form an ionic space charge layer due to the difference in electrostatic potential.^{54,55} If the Schottky barrier is high the Fermi energy at the interface will be lower than in the bulk, at least in the early stages of the experiments where the conductivity is not too low. Assuming a potential difference of 0.5 V and, for simplicity, Boltzmann statistics, the concentration of oxygen vacancies at the interface will be enhanced compared to that in the bulk by $\exp(0.5 \text{ eV} / k_B T)$, which amounts to $\sim 10^5$ at 200 °C. With such a high oxygen vacancy concentration, the space charge region at the electrode interface will become narrow enough that tunnelling can provide an ohmic contact.¹⁴ This does not conflict with rectifying current-voltage

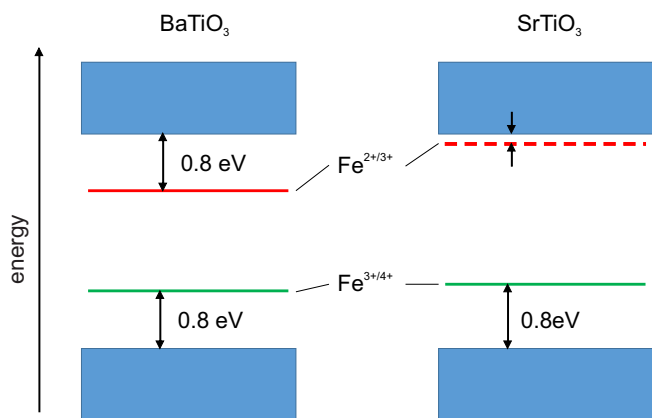


Fig. 8 Energetic positions of the $\text{Fe}^{3+/4+}$ - and $\text{Fe}^{2+/3+}$ -transition levels within the band gaps of BaTiO_3 and SrTiO_3 . The conduction and valence band of two materials are almost aligned, which is derived from photoelectron spectroscopy.^{13,53,60}

curves obtained with Pt contacts on Nb-doped SrTiO_3 .^{56,57} as oxygen vacancies are minority defects in Nb-doped SrTiO_3 .⁵⁸ The presence of ohmic contacts, despite nominally high Schottky barriers, has also been observed for SnO_2 .⁵⁹ In this case, the absence of electron blocking interfaces has been related to the large contact area and to charge transport only along small parts such as grain boundaries. Grain boundaries are excluded in the present situation but dislocations may also contribute to the formation of an ohmic contact.

The energy levels of the $\text{Fe}^{3+/4+}$ - and the $\text{Fe}^{2+/3+}$ -transition are illustrated in Fig. 8. According to literature, the energy levels of transition-metal impurities in different materials are aligned if the energy bands are arranged according to their energy band alignment. This has been particularly demonstrated for III-V semiconductors.^{20–22} As shown in Fig. 8, the valence band maxima of SrTiO_3 and BaTiO_3 are very close in energy. This has been derived from photoelectron spectroscopy studies^{13,53,60} and is reasonable according to the very similar electronic structures of both materials.^{13,60} Due to this, one could expect that the energy levels of the Fe impurity in SrTiO_3 and SrTiO_3 are also aligned. This is indeed the case for the $\text{Fe}^{3+/4+}$ -transition, which is 0.8–0.9 eV above the valence band maximum in both materials. In contrast, the $\text{Fe}^{2+/3+}$ -transition in BaTiO_3 is ~ 0.8 eV below the conduction band minimum, while it is close to the conduction band minimum in SrTiO_3 . The difference could be related to the ionic radius of Fe^{2+} , which is slightly larger than that of Ti^{4+} . While the larger Ba ion leaves more space in the center of the oxygen octahedra to accommodate a larger cation, an Fe^{2+} ion might induce a substantial lattice relaxation in SrTiO_3 . However, additional studies are required to resolve the origin of the higher energy of the $\text{Fe}^{2+/3+}$ -transition in SrTiO_3 .

5 Summary and Conclusions

An approach to determine the energy levels of defects in high-permittivity dielectrics from the observation of the activation energy of electronic transport in the course of stepwise oxidation of reduced crystals has been presented. Nominally undoped BaTiO_3 single crystals containing $3 \cdot 10^{17} \text{ cm}^{-3}$ Fe impurities and

0.05 wt.% Fe-doped SrTiO_3 single have been studied. The conductivity is measured in parallel plate geometry with Pt electrodes and using direct current. The applied voltage was kept low in order to avoid polarization of the samples.

After reduction, the samples contained oxygen vacancy concentrations slightly higher than the Fe concentration, making them n-type electronic conductors. The samples were slowly heated in N_2/O_2 atmosphere up to temperatures where the conductivity starts to decrease by oxygen incorporation and cooled down again after a certain holding time. This allows for a controlled slow re-oxidation of the samples. A homogeneous vacancy distribution is enabled by a high thermodynamic factor for oxygen diffusion, as the oxygen vacancy concentration is close to the Fe concentration.

A contribution of ionic transport to the measurements can clearly be excluded in the case of SrTiO_3 and is also not likely to affect the measurement in the case of BaTiO_3 . The study reveals a plateau of the activation energy at ~ 0.8 eV for BaTiO_3 . In the context of defect models provided in literature, this energy level can be associated to the $\text{Fe}^{2+/3+}$ -transition of the Fe impurity. In contrast, the conductivity of Fe-doped SrTiO_3 abruptly changes from n-type with a temperature independent carrier concentration to p-type behaviour with a high activation energy. This rules out the presence of a $\text{Fe}^{2+/3+}$ -transition at an energy substantially below the conduction band minimum. Very likely, that transition is energetically located near the conduction band minimum. While the energy level of the $\text{Fe}^{3+/4+}$ -transition is at similar energy in BaTiO_3 and SrTiO_3 , this rule does not hold for the $\text{Fe}^{2+/3+}$ -transition. The origin of the higher energy of the $\text{Fe}^{2+/3+}$ -transition in SrTiO_3 is not clear at present. Lattice relaxations might contribute to the effect.

According to the presented results, it seems unlikely that the electron trap observed in impedance studies in the cathode region of degraded Fe-doped SrTiO_3 ³⁷ is caused by the $\text{Fe}^{2+/3+}$ -transition. Moreover, due to the different defect energy levels, acceptor-doped SrTiO_3 cannot generally be used as a model system for studying degradation behaviour of high-permittivity dielectrics.

Acknowledgement

Issei Suzuki has been financially supported by an Overseas Research Fellowship of the Japanese Society for the Promotion of Science (JSPS). Support from the U.S. Air Force Office of Scientific Research under contract number FA9550-14-1-0158 is gratefully acknowledged. We also like to thank Roger A. de Souza for helpful discussions.

References

- 1 T. Baiatu, R. Waser and K.-H. Härdtl, *J. Am. Ceram. Soc.*, 1990, **73**, 1663–1673.
- 2 J.-J. Wang, H.-B. Huang, T. J. M. Bayer, A. Moballegh, Y. Cao, A. Klein, E. C. Dickey, D. L. Irving, C. A. Randall and L.-Q. Chen, *Acta Mater.*, 2016, **108**, 229–240.
- 3 H. Kishi, Y. Mizuno and H. Chazono, *Jpn. J. Appl. Phys.*, 2003, **42**, 1–15.
- 4 C. A. Randall, R. Maier, W. Qu, K. Kobayashi, K. Morita,

- Y. Mizuno, N. Inoue and T. Oguni, *J. Appl. Phys.*, 2013, **113**, 014101.
- 5 J. Watson and G. Castro, *J. Mater. Sci.: Mater. Electron.*, 2015, **26**, 9226–9235.
- 6 A. Zeb and S. J. Milne, *J. Mater. Sci.: Mater. Electron.*, 2015, **26**, 9243–9255.
- 7 J. Rödel and G. Tomandl, *Journal of Materials Science*, 1984, **19**, 3515–3523.
- 8 S. Rodewald, N. Sakai, K. Yamaji, H. Yokokawa, J. Fleig and J. Maier, *J. Electroceram.*, 2001, **7**, 95–105.
- 9 G. Y. Yang, E. C. Dickey, C. A. Randall, D. E. Barber, P. Pinceloup, M. A. Henderson, R. A. Hill, J. J. Beeson and D. J. Skamser, *J. Appl. Phys.*, 2004, **96**, 7492–7499.
- 10 W. Liu, G.-Y. Yang and C. A. Randall, *Jpn. J. Appl. Phys.*, 2009, **48**, 051404.
- 11 R. Giesecke, R. Hertwig, T. Bayer, C. A. Randall and A. Klein, *J. Am. Ceram. Soc.*, 2017, **100**, 4590–4601.
- 12 R. A. De Souza, *Adv. Funct. Mater.*, 2015, **25**, 6326–6342.
- 13 A. Klein, *J. Am. Ceram. Soc.*, 2016, **99**, 369–387.
- 14 S. M. Sze and K. K. Ng, *Physics of Semiconductor Devices*, John Wiley & Sons, Hoboken, 2007.
- 15 D. K. Schroder, *Semiconductor material and device characterization*, John Wiley & Sons, Hoboken, 2006.
- 16 C. N. Berglund and W. S. Baer, *Phys. Rev.*, 1967, **157**, 358–366.
- 17 H.-J. Hagemann, *PhD thesis*, RWTH Aachen, 1980.
- 18 O. N. Tufte and P. W. Chapman, *Phys. Rev.*, 1967, **155**, 796–802.
- 19 R. Moos, W. Menesklou and K. H. Härdtl, *Appl. Phys. A*, 1995, **61**, 389–395.
- 20 M. J. Caldas, A. Fazzio and A. Zunger, *Appl. Phys. Lett.*, 1984, **45**, 671–673.
- 21 A. Zunger, *Phys. Rev. Lett.*, 1985, **54**, 849.
- 22 J. M. Langer and H. Heinrich, *Phys. Rev. Lett.*, 1985, **55**, 1414–1417.
- 23 S. S. Hegedus and W. N. Shafarman, *Prog. Photovolt. Res. Appl.*, 2004, **12**, 155–176.
- 24 H.-J. Hagemann and D. Hennings, *J. Am. Ceram. Soc.*, 1981, **64**, 590–594.
- 25 M. B. Klein and R. N. Schwartz, *J. Opt. Soc. Am. B*, 1986, **3**, 293–305.
- 26 E. Possenriede, O. F. Schirmer, H. J. Donnerberg, G. Godefroy and A. Maillard, *Ferroelectrics*, 1989, **92**, 245–252.
- 27 B. A. Wechsler and M. B. Klein, *J. Opt. Soc. Am. B*, 1988, **5**, 1711–1723.
- 28 M. B. Klein, *Photorefractive Materials and Applications 2: Materials*, Springer, New York, 2007, pp. 241–284.
- 29 I. Denk, W. Münch and J. Maier, *J. Am. Ceram. Soc.*, 1995, **78**, 3265–3272.
- 30 R. Moos and K. H. Härdtl, *J. Am. Ceram. Soc.*, 1997, **80**, 2549–2562.
- 31 R. A. Maier and C. A. Randall, *J. Am. Ceram. Soc.*, 2016, **99**, 3350–3359.
- 32 R. A. Maier and C. A. Randall, *J. Am. Ceram. Soc.*, 2016, **99**, 3360–3366.
- 33 A. Mazur, O. F. Schirmer and S. Mendricks, *Appl. Phys. Lett.*, 1997, **70**, 2395–2397.
- 34 V. G. Bhide and H. C. Bhasin, *Phys. Rev.*, 1968, **172**, 290–294.
- 35 C. T. Luiskutty and P. J. Ouseph, *Solid State Commun.*, 1973, **13**, 405–409.
- 36 R. B. Comes, T. C. Kaspar, S. M. Heald, M. E. Bowden and S. A. Chambers, *J. Phys.: Condens. Matter*, 2016, **28**, 035901.
- 37 T. J. M. Bayer, J. J. Carter, J.-J. Wang, A. Klein, L.-Q. Chen and C. A. Randall, *J. Appl. Phys.*, 2017, **122**, 244101.
- 38 C. G. V. de Walle and J. Neugebauer, *Nature*, 2003, **423**, 626–628.
- 39 C. Linderälv, A. Lindman and P. Erhart, *J. Phys. Chem. Lett.*, 2018, **9**, 222–228.
- 40 H.-I. Yoo, C.-R. Song and D.-K. Lee, *J. Electroceram.*, 2002, **8**, 5–36.
- 41 P. Erhart and K. Albe, *J. Appl. Phys.*, 2008, **104**, 044315.
- 42 H.-I. Yoo, T.-S. Oh, H.-S. Kwon, D.-K. Shin and J.-S. Lee, *Phys. Chem. Chem. Phys.*, 2009, **11**, 3115–3126.
- 43 H. Ihrig, *J. Phys. C: Solid St. Phys.*, 1976, **9**, 3469.
- 44 M. Kessel, R. A. De Souza and M. Martin, *Phys. Chem. Chem. Phys.*, 2015, **17**, 12587–12597.
- 45 N. H. Chan, R. K. Sharma and D. M. Smyth, *J. Am. Ceram. Soc.*, 1981, **64**, 556–562.
- 46 D. M. Long, A. Klein and E. C. Dickey, *Appl. Surf. Sci.*, 2019, **466**, 472–476.
- 47 T. Inoue, N. Seki, J. Kamimae, K. Eguchi and H. Arai, *Solid State Ionics*, 1991, **48**, 283–288.
- 48 F. Chen and A. Klein, *Phys. Rev. B*, 2012, **86**, 094105.
- 49 J. Maier, *J. Am. Ceram. Soc.*, 1993, **76**, 1223–1227.
- 50 T. Bieger, J. Maier and R. Waser, *Solid State Ionics*, 1992, **53**, 578–582.
- 51 J. N. Baker, P. C. Bowes, D. M. Long, A. Moballegh, J. S. Harris, E. C. Dickey and D. L. Irving, *Appl. Phys. Lett.*, 2017, **110**, 122903.
- 52 R. Schafraneck, S. Payan, M. Maglione and A. Klein, *Phys. Rev. B*, 2008, **77**, 195310.
- 53 S. Balaz, Z. Zeng and L. J. Brillson, *J. Appl. Phys.*, 2013, **114**, 183701.
- 54 J. Maier, *Prog. Solid-St. Chem.*, 1995, **23**, 171–263.
- 55 J. Maier, *Physical Chemistry of Ionic Materials*, Wiley-VCH, Weinheim, 2004.
- 56 J. Li, N. Ohashi, H. Okushi and H. Haneda, *Phys. Rev. B*, 2011, **83**, 125317.
- 57 S. Hirose, H. Yoshikawa, H. Yanagi, A. Ando, S. Ueda and N. Ohashi, *ECS J. Solid State Sci. Technol.*, 2014, **3**, 243–248.
- 58 R. Meyer, A. F. Zurhelle, R. A. D. Souza, R. Waser and F. Gunkel, *Phys. Rev. B*, 2016, **94**,
- 59 C. Körber, S. P. Harvey, T. O. Mason and A. Klein, *Surf. Sci.*, 2008, **602**, 3246–3252.
- 60 S. Li, F. Chen, R. Schafraneck, T. J. M. Bayer, K. Rachut, A. Fuchs, S. Siol, M. Weidner, M. Hohmann, V. Pfeifer, J. Morasch, C. Ghinea, E. Arveux, R. Günzler, J. Gassmann,

C. Körber, Y. Gassenbauer, F. Säuberlich, G. V. Rao, S. Payan, M. Maglione, C. Chirila, L. Pintilie, L. Jia, K. Ellmer, M. Naderer, K. Reichmann, U. Böttger, S. Schmelzer, R. C.

Frunza, H. Uršič, B. Malič, W.-B. Wu, P. Erhart and A. Klein, *phys. stat. sol. (rrl)*, 2014, **8**, 571–576.